Title
COMPARISON OF AN INCLUSIVE MULTIPERIPHERAL MODEL TO SECONDARY SPECTRA IN p-p COLLISIONS

Authors
Risk, Clifford
Friedman, Jerome H.

Publication Date
1971-03-01

Submitted to
Physical Review Letters

C. Risk

UCRL-20199
Preprint

C.2

COMPARISON OF AN INCLUSIVE MULTIPERIPHERAL MODEL TO SECONDARY SPECTRA IN p-p COLLISIONS

Clifford Risk and Jerome H. Friedman

March 1971

AEC Contract No. W-7405-eng-48

DISCLAIMER

COMPARISON OF AN INCLUSIVE MULTIPERIPHERAL MODEL TO SECONDARY SPECTRA IN p-p COLLISIONS*

Clifford Risk

Lawrence Radiation Laboratory
University of California
Berkeley, California 94720

and

Department of Physics
University of California
Davis, California 95616

and

Jerome H. Friedman

Lawrence Radiation Laboratory
University of California
Berkeley, California 94720

March 1971

ABSTRACT

The quantitative predictions of an inclusive multiperipheral model are compared to the measured secondary spectra in pp collisions from 12 to 30 GeV/c.

For proton-proton collisions at high energies the dominant contributions to the total cross section come from inelastic processes. The simplest probe of these processes are inclusive experiments of the type $pp \to x + \text{anything}$ where x is one of the several types of final-state particles (e.g., $\pi^{\pm}$, $K^{\pm}$, or p). The usual procedure is to measure the momentum spectra of x for various angles of its

production. Recently, three such experiments have been performed at 12.4,[1] 19.2,[2] and 30[3] GeV/c. In this report we show that the prominent characteristics of these spectra can be understood with a simple multiperipheral model that contains the known properties of two-body scattering processes. We compare the $\pi^{\pm}$, $K^{\pm}$, and proton spectra measured by these experiments to the predictions of an inclusive multiperipheral model that is a modified version of that first proposed by Caneschi and Pignotti[4] (CP).

Our modified Caneschi and Pignotti inclusive multiperipheral model (MCP) is illustrated by the diagrams of Fig. 1. Figure 1a represents the case where the proton remains at the end of the multiperipheral chain, Fig. 1b represents the baryon exchange case where the proton travels down one link, emitting a pion at the end of the chain, and Fig. 1c characterizes the pions produced at the internal links. In all three cases the remaining links in the multiperipheral chain are simulated by the inelastic scattering of an exchanged meson, m, with the remaining incident protons.

For all three diagrams the exchanged meson trajectories are chosen to be the same, and are set equal to the absorbed ρ-meson trajectory given by Berger and Fox.[5] The exchanged baryon trajectories are represented by the known s and t dependence of the backward meson-baryon elastic scattering.[6] The energy dependence of the exchanged meson-baryon total cross section is taken, in all three diagrams, to be slowly falling from threshold to an asymptotically constant value. Specifically, $\sigma_T(M^2) = 24(1 + 0.3/M^2)$. The two residue functions, $\beta_m(t)$ and $\beta_B(t)$, associated with the meson and baryon exchanges, respectively, are taken to be functions only of the corresponding four-momentum transfers squared. These functions are adjusted

(as described below) to give the best correspondence to the experimental data.

This model (MCP) primarily differs from (CP) in that the fast mesons and slow protons are described by a single diagram (Fig. 1b) instead of the three diagrams used by (CP). This eliminates the need for extrapolating the $\bar{p}p$ total cross section below threshold.

As derived by (CP) on the basis of multi-Reggeism the matrix elements squared for the processes corresponding to the diagrams of Figs. 1abc can be expressed, respectively, as

$$R_1 = (S/M^2)^{2\alpha_m(t)}\, \beta_m{}^2(t)\, M^2\, \sigma_T(M^2)$$

$$R_2 = S_1^{2\alpha_B(t_1)} (S_2/M^2)^{2\alpha_m(t_2)}\, \beta_B{}^2(t_1)\, \beta_m{}^2(t_2)\, M^2\, \sigma_T(M^2)$$

$$R_3 = \left(\frac{S_1}{M_1{}^2}\right)^{2\alpha_m(t_1)} \left(\frac{S_2}{M_2{}^2}\right)^{2\alpha_m(t_2)} \beta_m{}^2(t_1)\, \beta_m{}^2(t_2)\, M_1{}^2\, \sigma_T(M_1{}^2) \times M_2{}^2\, \sigma_T(M_2{}^2).$$

This model is obviously a crude approximation to a genuine multiperipheral model. Its principal advantage is calculational ease, since to describe these multiparticle final states only three-body space integrals (at most) need to be evaluated. The crudeness of this model precludes a definitive and unambiguous comparison of theory with experiment. The best that one can hope to achieve is a consistent explanation of the various experimental results within a physically viable model that reproduces the salient features of the spectra. It is in this spirit that we perform such a comparison.

To describe the data with our model we use the following procedure. We adjust the meson-exchange residue function, $\beta_m(t)$, to best describe the shape of the pion transverse momentum squared, $p_T{}^2$, spectrum at the smallest longitudinal momentum, p_L, measured in the

12.4 GeV/c data of Ref. 1. We find $\beta_m{}^2(t)$ equal to $e^{2.1t}$ for $t > -0.3$, and $c\, e^{0.3t}$ for $t < -0.3$. We adjust the baryon-exchange residue function, $\beta_B(t)$, to best describe the $p_T{}^2$ dependence of the pions with large p_L using the 19.2 GeV/c data of Ref. 2. We obtain $\beta_B{}^2(t)$ equal to $e^{1.5t}$ for $t > 0.2$ and $c'\, e^{0.2t}$ for $t < 0.2$. Here the constants c and c' are inserted simply to insure continuity.

We normalize the contribution of the process diagrammed in Fig. 1a to reproduce the magnitude of the fast (large p_L) protons and that of Fig. 1b to reproduce the magnitude of the fast pions, both at 19.2 GeV/c. The contribution of the process diagrammed in Fig. 1c is normalized to the magnitude of the slow (small p_L) pions at 12.4 GeV/c. The complete π^+, π^- and proton spectra are now predicted at all three energies. We now discuss the salient features of these measured spectra and their description in terms of this model.

(1) The proton spectra.

The process diagrammed in Fig. 1a gives rise to elastic forward produced protons and hence a sharp peaking in the proton $p_T{}^2$ spectra. The process of Fig. 1b gives rise to more inelastic larger angle protons. This is a consequence of the proton emitting a pion before scattering from the other incident proton and hence emerging on the average at a larger angle and lower momentum than the single scattered protons of Fig. 1a. Therefore this model predicts that the $p_T{}^2$ distribution will become more sharply peaked at larger longitudinal momentum, a result confirmed by the experimental data. Specifically, in the center of mass this implies that factorization of the cross section $d^2\sigma/(d^3p/E) = f_1(p_T{}^2)\, f_2(p_L)$ does not hold.

The protons with large longitudinal momentum arising from the process of Fig. 1a describe the background to the structure observed near the kinematical limit at 19.2 and 30 GeV/c (Figs. 2bc). This structure could have been reproduced with our model by including the low-energy resonances in the meson-proton total cross section, $\sigma_T(M^2)$. Figure 2 compares the predictions of our model to the measured proton spectra.

(2) Pion transverse momentum spectra.

Figure 3a displays the p_T^2 spectra of the π^+ and π^- at 12.4 GeV/c as measured by Ref. 1. These distributions are both characterized by a striking peak ($e^{-15\ p_T^2}$) for small p_T^2 that levels off to a more gentle dependence ($e^{-3\ p_T^2}$) for larger p_T^2. In our model the sharp peaking results from two mechanisms. The first comes from the forward pions produced at the end of the multiperipheral chain in the baryon-exchange process of Fig. 1b and is similar to the mechanism that produces the sharp peaking in the proton p_T^2 spectra. The second mechanism comes from the pions produced with very small longitudinal momentum in the process of Fig. 1c. These pions result when the missing masses M_1 and M_2 are approximately equal; or in analogy with a genuine multiperipheral model, these are the pions produced near the center of the chain. The more slowly falling part of the spectrum for larger p_T^2 arises from the pions produced at intermediate links in the multiperipheral chain in a manner similar to the mechanism that produces the slower larger angle protons. In terms of Fig. 1c this occurs when M_1 and M_2 have dissimilar values.

(3) Pion longitudinal momentum spectra.

The data at 12.4 and 19.2 GeV/c (Refs. 1 and 2) shows the π^- spectrum falling much more rapidly at large values of p_L than the π^+

(Figs. 2bcd). For the 19.2 GeV/c data, in the interval from p = 10 to 16 GeV/c the π^- rate decreases five times faster than the π^+ rate. In our model this arises from the difference between π^-p and π^+p backward elastic scattering in the process of Fig. 1b. The backward π^-p elastic cross section falls faster from the resonance region than the corresponding π^+p cross section.[7] In our model the very fastest pions result from the case where the πp subenergy s_1 (Fig. 1b) is large. Therefore the relative smallness of the π^-p as compared to the π^+p backward elastic cross sections for these large subenergies ($s_1 \sim 10$ GeV^2) results in the relative depletion of the π^- with large p_L. Figures 3(a-e) compare the predictions of our model to the measured $\pi^\pm$ spectra.

(4) The $K^\pm$ spectra.

The relation imposed by this model between fast meson secondaries and the meson-proton backward elastic scattering cross section should be even more pronounced for the $K^\pm$ spectra than the $\pi^\pm$ spectra. This is because backward K^-p scattering at large energy involves exotic exchange while K^+p does not, and hence the K^-p backward elastic cross section falls with increasing energy much more rapidly than the backward K^+p.[8] In our model the absence of exotic exchanges implies that only the process corresponding to Fig. 1c can contribute to the K^- spectrum while those of both Figs. 1b and 1c can contribute to the K^+ spectrum.

To describe the K spectra we use the same trajectories and residue functions found to best describe the $\pi^\pm$ and p spectra. We adjust the normalization of the contribution of the process diagrammed in Fig. 1c to give the best overall normalization to the K^- spectra and normalize the contribution of Fig. 1b to the fast K^+

spectrum. Figures 3f and 3g compare the predictions of this model to the K^+ and K^- spectra at 19.2 GeV/c. The lack of fast K^- relative to K^+ is apparent in the measured spectra and is adequately described by our model.

To summarize, we have compared the quantitative predictions of a fairly restrictive inclusive multiperipheral model to the meson and proton spectra resulting from pp collisions at three momenta from 12 to 30 GeV/c. The model adequately describes the particle spectra by relating them to the well-known properties of two-body scattering processes.

There are some discrepancies between the predictions of our model and the measured spectra. In particular our model gives not enough peaking in the p_T^2 distribution for $p_T^2 \leq 0.05$ $(GeV/c)^2$ in the 12.4 GeV/c data (Fig. 3a). Also, for large p_T^2 our model predicts too small a cross section for the $\pi^\pm$ spectra at 12.4 GeV/c and the proton spectra at 12.4 and 30 GeV/c. These as well as various other discrepancies could perhaps be reduced by further adjustment of the residue functions $\beta_m(t)$ and $\beta_B(t)$. However, this model is such a crude approximation to a detailed multiperipheral model that very little more insight into the dynamics of these processes can be obtained by pursuing the model beyond its scope.

The dependence of particle spectra on two-body scattering characteristics has also been incorporated into the limiting fragmentation approach.[9] There, by invoking general concepts such as reversal of the line of flight of a charge, qualitative predictions can be made on the structure of secondary spectra that are similar to our results.

We express our gratitude to J. Ball, V. Chung, G. Kane, G. Lynch, G. Marchesini, and M. Ross for helpful discussions.

FOOTNOTES AND REFERENCES

* This work was supported in part by the U.S. Atomic Energy Commission.

1. C. W. Akerlof, et al., Phys. Rev. D3, 645 (1971).
2. J. V. Allaby, et al., CERN preprint 70-12, April, 1970 (unpublished).
3. E. W. Anderson, et al., Phys. Rev. Letters 19, 198 (1967).
4. L. Caneschi and A. Pignotti, Phys. Rev. Letters 22, 1219 (1969).
5. E. L. Berger and G. Fox, Argonne National Laboratory preprint ANL/HEP 7019, Aug. 1970 (unpublished).
6. S. W. Karmanyos, et al., Phys. Rev. Letters 16, 709 (1966).
7. M. Derrick, Proceedings of the Topical Conference on High Energy Collisions of Hadrons, CERN Report CERN 68-7 Vol. 1, p. 111, Feb. 1968 (unpublished).
8. W. F. Baker, et al., Nucl. Phys. B25, 385 (1971).
9. T. T. Chou and C. N. Yang, Phys. Rev. Letters 25, 1072 (1970).

FIGURE CAPTIONS

Fig. 1. Diagrams representing the processes comprising the inclusive multiperipheral model described in the text.

Fig. 2. Proton spectra measured at (a) 12.4 GeV/c (Ref. 1), (b) 19.2 GeV/c (Ref. 2), and (c) 30 GeV/c (Ref. 3). The solid lines are the predictions of the model.

Fig. 3. Meson spectra. (a,b) $\pi^\pm$ at 12.4 GeV/c (Ref. 1), (c,d) $\pi^\pm$ at 19.2 GeV/c (Ref. 2), (e) $\pi^\pm$ at 30 GeV/c (Ref. 3), and (f,g) $K^\pm$ at 19.2 GeV/c (Ref. 2). The solid lines are the predictions of the model.

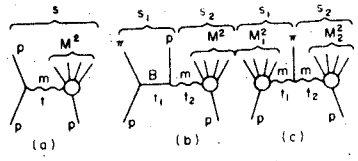

Fig. 1.

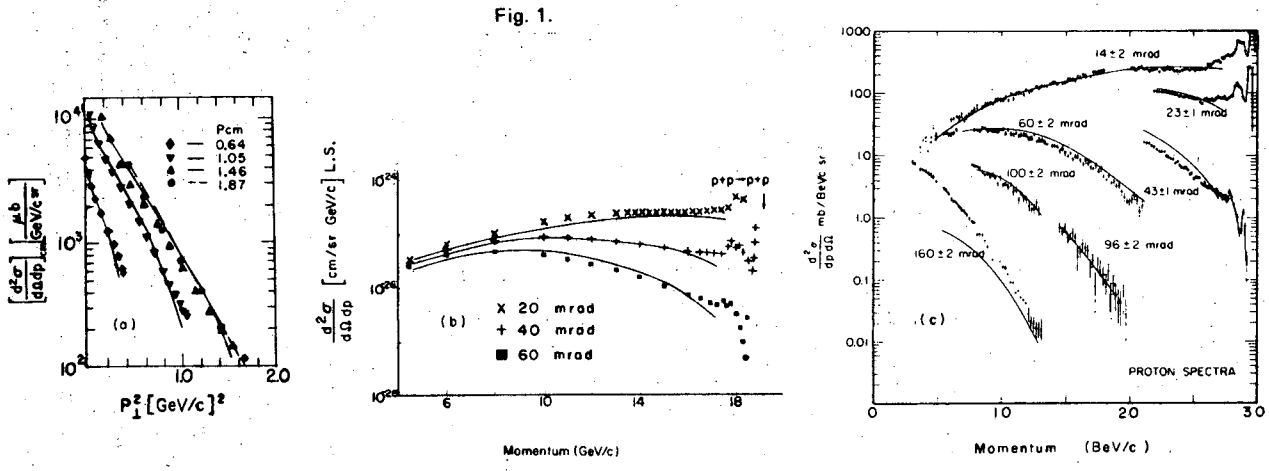

Fig. 2

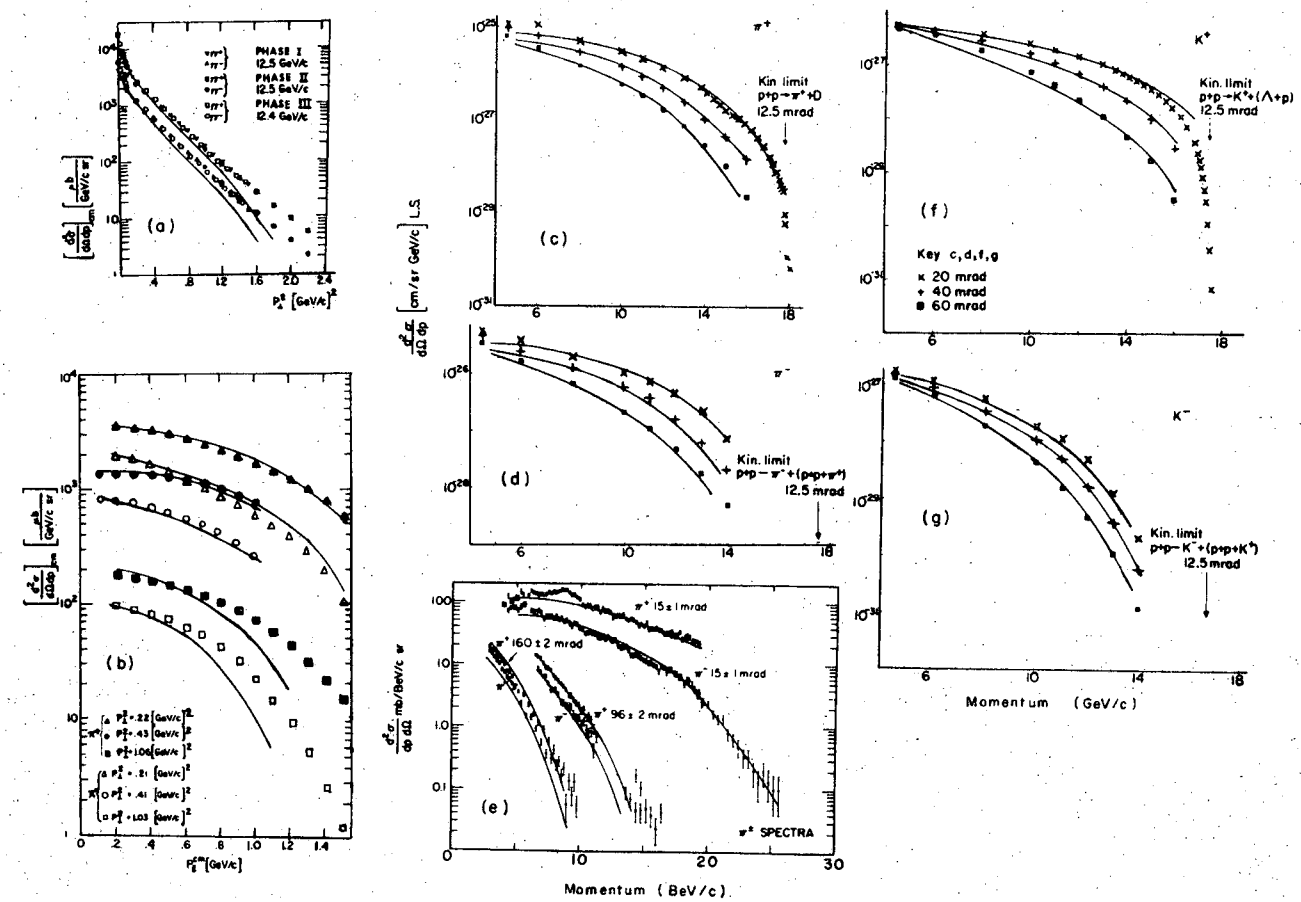

Fig. 3.

TECHNICAL INFORMATION DIVISION
LAWRENCE RADIATION LABORATORY
UNIVERSITY OF CALIFORNIA
BERKELEY, CALIFORNIA 94720